Original article

Desmoglein-3 acts as a pro-survival protein by suppressing reactive oxygen species and doming whilst augmenting the tight junctions in MDCK cells

Xiao Li[a1], Usama Sharif Ahmad[a1], Yunying Huang[a], Jutamas Uttagomol[a], Ambreen Rehman[a], Ke Zhou[c], Gary Warnes[b], Simon McArthur[a], Eric Kenneth Parkinson[a] and H Wan[a*]

[a]*Centre for Immunobiology and Regenerative Medicine Institute of Dentistry and* [b]*Blizard Institute, Barts and The London, School of Medicine and Dentistry, Queen Mary University of London, UK;* [c]*CB Joint MHNCRL, Hospital and School of Stomatology, Guizhou Medical University, China.*

[1] These authors contributed equally to this work.

To whom correspondence should be addressed. E-mail: *h.wan@qmul.ac.uk*

***Dr. Hong Wan BDS, MSc, PhD**
Centre for Immunobiology and Regenerative Medicine
Institute of Dentistry
Barts and The London, School of Medicine and Dentistry
Queen Mary University of London
4 Newark Street, Whitechapel
London E1 2AT
Tel: 0044 (0) 20 7882 7139
Fax: 0044 (0) 20 7882 7137
E-mail: *h.wan@qmul.ac.uk*
ORCID iD: orcid.org/0000-0003-3794-5692

Funding sources: no external funding.

The authors declare no conflict of interest.

Abstract

Kidney disease prevalence increases with age, with a common feature of the disease being defects in the epithelial tight junctions. Emerging evidence suggests that the desmosomal adhesion protein Desmoglein-3 (Dsg3) functions beyond the desmosomal adhesion and plays a role in regulating the fundamental pathways that govern cell fate decisions in response to environmental chemical and mechanical stresses. In this study, we explored the role of Dsg3 on dome formation, reactive oxygen species (ROS) production and transepithelial electrical resistance (TER) in MDCK cells, a kidney epithelial cell model widely used to study cell differentiation and tight junction formation and integrity. We show that overexpression of Dsg3 constrained nuclear ROS production and cellular doming in confluent cell cultures and these features coincided with augmented TER and enhanced tight junction integrity. Conversely, cells expressing dominant-negative Dsg3ΔC mutants exhibited heightened ROS production and accelerated doming, accompanied by increased apoptosis, as well as cell proliferation, with massive disruption in F-actin organization and accumulation and alterations in tight junctions. Inhibition of actin polymerization and protein synthesis was able to sufficiently block dome formation in mutant populations. Taken together, these findings underscore that Dsg3 has a role in controlling cellular viability and differentiation as well as the functional integrity of tight junctions in MDCK cells.

Keywords: Desmoglein; actin cytoskeleton; ROS; dome formation; tight junction; TER; transepithelial permeability; MDCK cells.

1. **Introduction**

The prevalence of end-stage renal disease increases almost exponentially in parallel with chronological age (Stewart et al., 2006). Chronic kidney disease is estimated to affect more than 30-40% of humans around the age of 70 and 50% of those around 80 in the U.S.A (Grams et al., 2013,Coresh et al., 2005) and is emerging as a considerable burden to health service providers. Renal epithelial tight junction (TJ) barrier function has been shown to be compromised during aging. Indeed, age-related increased changes in TJ integrity have been reported (Haddad et al., 2005,Reyes et al., 2002).

The Madin-Darby Canine Kidney (MDCK) cell lines are widely used as epithelial models to study TJs, cell polarity, and epithelial differentiation and morphogenesis. Early studies (in the 1970s) showed that MDCK cells spontaneously develop domes under specific conditions in confluent cultures of approximately two weeks age (Rothen-Rutishauser et al., 1998,Lever, 1979a). Domes are structures of fluid-filled multicellular hemicysts or blisters resulting from local accumulations of sodium and water beneath the cell monolayer due to the fluid-transporting nature of these simple epithelial cells (Kennedy and Lever, 1984,Leighton et al., 1970). It has been reported that domes can be induced by compounds such as hexamethylene bis acetamide (HMBA) and dimethylformamide (DMF) that are known to induce cell differentiation (Kennedy and Lever, 1984,Leighton et al., 1970,Oberleithner et al., 1990), and therefore dome formation is regarded as a feature of ageing or differentiation. Ion transporters such as Na^+/K^+-ATPase and cAMP which are involved in regulating epithelial transmembrane transport, and Stat3 signaling that induces NHE3 expression, are independently implicated in promoting dome formation in MDCK cell lines (Su et al., 2007,Sugahara et al., 1984,Lever, 1979b,Lever, 1979a). However, what changes in TJs and the associated functions remain largely unknown. There are two major strains of MDCK cells, MDCK I and MDCK II. While the former exhibits the “tight” junction phenotype with high TER values (>1000 $\Omega \cdot cm^2$), the latter, *i.e.* MDCK II cell line possesses a ‘leaky’ phenotype with much lower TER values (<300 $\Omega \cdot cm^2$) and is the most commonly used MDCK strain for studying epithelial cell biology including dome formation (Dukes et al., 2011).

The desmosomal cadherin Desmoglein-3 (Dsg3) is a member of cadherin superfamily and mediates cell-cell adhesion in desmosomes, in a calcium-dependent manner, in vertebrate epithelial cells. This protein is predominantly expressed in stratified epithelia with reduced levels in simple epithelial cells such as MDCK cells as well as in many cancer lines of immortal status (Tsang et al., 2012a,Brown et al., 2014,Tsang et al., 2010,Teh et al., 2011). In fact, Dsg3 is found to be present along the entire plasma membrane and not just restricted within the desmosomal plaque. Accumulating evidence suggests that Dsg3 does not solely function in desmosome adhesion and also exerts a signaling role for various intracellular pathways in epithelial cells, almost all of which are involved in the regulation of the actin cytoskeleton that affects cell adhesion, shape change and motility (Brown and Wan, 2015,Brown et al., 2014,Tsang et al., 2010,Tsang et al., 2012b,Tsang et al., 2012a). Our previous study has shown that overexpression of Dsg3 in MDCK cells promotes actin dynamics and turnover (Tsang et al., 2012a). However, it remains unclear whether this phenomenon has any impact on cell properties such as longevity and ageing. Many studies on Dsg3 in the literature have focused on the pathogenesis of pemphigus autoimmune disease in which Dsg3 serves as a major antigen (*pemphigus vulgaris* antigen, PVA) (Amagai et al., 1991). Recent studies have revealed that Dsg3 is upregulated in cancer and exhibits a pro-cancerous role by activating various

signaling pathways, such as Src, Rac1/Cdc42, Ezrin and AP-1, that are known to be hijacked in cancer and are involved in regulating various processes, including junction remodeling, E-cadherin adhesion and trafficking, cell proliferation and motility (Moftah et al., 2016,Brown and Wan, 2015). Although the biological function of Dsg3 in desmosome adhesion is well established, the non-junctional role for Dsg3 remains an area of active research.

In this study, we investigated the effect of overexpression of wild type or C-terminally truncated Dsg3 on dome formation, ROS production and tight junction integrity (TER and paracellular permeability) in MDCK cells (MDCK II strain). We provide evidence that ectopic expression of wild type Dsg3 in MDCK cells protected against ROS production and apoptosis, facilitated the development of TJs and restricted dome formation. Conversely, opposite effects were detected in mutant cells expressing dominant-negative Dsg3ΔC constructs, with a phenotype of premature cell ageing, such as enhanced ROS production and apoptosis, altered cytoskeletal organization, and accelerated doming. Concomitantly, defects in TJs were shown in mutant cells. In summary, these findings underscore an important biological function for Dsg3 in control of epithelial cell well-being and longevity in MDCK cells.

2. Materials and methods

2.1. Cell Culture and antibodies

The Madin-Darby Canine Kidney (MDCK) strain II cells were used in this study and were maintained routinely in Dulbecco's Modified Eagle Medium (DMEM) supplemented with 10% fetal calf serum (FCS). Media was changed twice a week in prolonged cultures. The mouse monoclonal antibody (Ab) 5H10 that binds to the N-terminus of Dsg3 and rat monoclonal anti-ZO-1 was purchased from Santa Cruz Biotechnology. Other antibodies were also purchased commercially, *i.e.* anti-Ki67 (M7240, Dako), anti-cleaved caspase-3 (ab49822, Abcam), Claudin Antibody Sample Pack (900900, Invitrogen), cyclin A (sc-751, Santa Cruz) and PC10, mouse Ab to PCNA (sc-56, Santa Cruz). Alexa Fluor 488 conjugated rabbit Ab to non-muscle myosin IIa (ab204675, Abcam). Alexa Fluor 488 conjugated phalloidin and secondary Abs, Alexa Fluor 488/568 conjugated goat anti-mouse or anti-rat IgGs were purchased from Invitrogen. CellROX Oxidative Stress (Green) Reagent was supplied by Thermo Fisher Scientific. Senescence β-Galactosidase Staining Kit was purchased from BioVision (Cat #K802-250).

2.2. Generation of MDCK stable lines with transduction of full-length Dsg3 and its C-terminally truncated mutants

The retroviral construct of full-length human Dsg3 cDNA (pBABE-hDsg3.myc) and three C-terminally truncated constructs of Dsg3, tagged with a Myc epitope at C-terminus, were generated before in this laboratory (Tsang et al., 2010,Moftah et al., 2016). The generation of stable MDCK cell lines with transduction of pBABE-hDsg3.myc (Dsg3-FL) and three C-terminally truncated mutants (pBABE-Dsg3Δ238, Dsg3Δ458 and Dsg3Δ560) were previously described (Tsang et al., 2010,Moftah et al., 2016).

2.3. Treatment of dispase and trypsin/EDTA

The prolonged confluent cultures were washed with PBS twice and then incubated in 2 ml PBS containing dispase II (2.4 U/ml, Invitrogen) or trypsin-EDTA (0.25%, Thermo Fisher Scientific), at 37°C for a few minutes until the dome cells were round and dissociated. Phase-contrast images were acquired immediately with a microscope CCD camera (Nikon TE2000-S).

2.4. Dome scoring

Dome scoring was performed using a light microscope for the cultures of different ages with 10 randomly selected microscope fields scored for the number of domes.

2.5. FACS analyses of Annexin V staining and cell cycle

Cells were harvested, pelleted and re-suspended in 400 μl of calcium-rich Annexin V buffer (BD, UK) and 2 μl of Annexin V-FITC (BD, UK) and incubated at RT for 20 min. DAPI (200 ng/ml) was then added to cells to indicate viability and 30,000 cells were analyzed on a BD FACSCanto II flow cytometer (BD, UK). Cells were classified as live (double negative), early apoptotic (Annexin V^{+ve}/$DAPI^{-ve}$), late apoptotic (Annexin V^{+ve}/$DAPI^{+ve}$) and necrotic (Annexin V^{-ve}/$DAPI^{+ve}$). For cell cycle analysis, cells were harvested and fixed in ice-cold 70% ethanol for 1 hour at 4°C. After washing twice in PBS, cells were incubated with RNAse and PI (50 μg/ml) for 15 min at RT. Cells (30,000) were analyzed on a BD FACSCanto II (BD, UK) with the PI Area and Width parameters set to LIN and the voltage adjusted to gate on single cells. Histograms of the PI-Area parameter allow the discrimination of the percentage Sub G_1 (indicating late apoptosis), G_1, S phase, and G_2/M.

2.6. Measurement of nuclear ROS

The cell reactive oxygen species (ROS) levels were determined by using the CellROX® Oxidative Stress Reagent, a green fluorescent probe designed to reliably measure ROS in live cells (Molecular Probe by Life Technologies). This reagent can permeate the plasma and nuclear membranes and is non-fluorescent or weakly fluorescent while in a reduced state. Upon oxidation, this reagent changes to fluorescent dye exhibiting strong fluorogenic signals that preferentially bind to DNA. Therefore, the signals are localized primarily in the nucleus and mitochondria and are detectable by fluorescence microscopy. Cell cultures were treated with CellROX® Oxidative Stress Reagent added into growth medium at a final concentration of 5 μM, alongside negative DMSO controls. Cells were incubated at 37°C for 30 minutes before fixation with 4% formaldehyde and permeabilized with 0.1% Triton prior to immunostaining with Dsg3 Ab 5H10. For the antioxidant treatment with phenyl-alpha-tert-butyl nitrone (PBN, Sigma-Aldrich) (Joseph et al., 1995), cells were seeded in triplicate wells before treated with PBN at a final concentration of 400μM in the growth medium, alongside DMSO control. The plate was incubated for 2 hours before the addition of CellROX® Green Reagent as described above.

2.7. Measurement of TER and transepithelial permeability of FITC-dextran

MDCK cells were counted and plated at confluent density ($2x10^6$ per well) on 6-well Transwell filters in growth medium in duplicate. At the indicated time points, TER was measured with a Millicell ERS-2 volt-ohm meter (Millipore, USA), and monolayer TER values (expressed as $\Omega \cdot cm^2$) were obtained by subtracting blank (cell-free) filter readings. Three values per well were obtained at different locations of monolayers for all cell lines at each time point. For transepithelial permeability assay with 70-kDa fluorescein isothiocyanate–dextran (FITC-dextran) (46945-100MG-F, Sigma), cells were seeded at confluent density in Transwell inserts with 12-well format and allowed to grow for two weeks with the medium changed every day. Permeability was measured from FITC-dextran (2mg/ml) across the MDCK monolayers at 3, 10 and 14 days, respectively, followed procedures described previously (Cristante et al., 2013). Briefly, 70-kDa FITC-dextran was prepared in transport buffer (DMEM w/o phenol red + 2% FCS) and was added to each filter insert, with only transport buffer being added to the lower wells. Filter inserts were incubated for 5 min and transported sequentially at 5 min intervals for 30 min. A standard curve was made by diluting the original 2mg/ml stock FITC-dextran at 1:1000, 1:5000 and 1:10,000. 100µl of the lower well medium was collected for each time point and transferred to a 96-well plate alongside 100µl of each standard curve point. The plate was read for fluorescence with excitation 485nm, emission 520nm, and 80% gain. Coefficients of permeability were calculated according to the formula: $1/P_{total} = 1/P_{endothelial} + 1/P_{filter}$ and expressed as $x10^{-3}$ $cm.min^{-1}$.

2.8. Fluorescent staining and confocal microscopy

Cultured cells grown on coverslips were fixed in 4% formaldehyde in PBS for 10 minutes and permeabilized with 0.1% Triton X-100 for 5 minutes. Non-specific binding sites were blocked with 10% goat serum for 20 minutes. Fluorescent staining was performed using the antibodies described above. All antibodies were diluted in 10% goat serum. Coverslips were washed three times with washing buffer (PBS containing 0.2% Tween 20) after each antibody incubation. Finally, coverslips were counterstained with DAPI for 8-10 minutes and were mounted on slides. Images of fluorescent staining were acquired on a Zeiss 710 LSM confocal microscope using a 63x/1.4 NA objective or a Leica DM4000 epifluorescence microscope using 40x/1.2 NA objective and analyzed with ImageJ.

2.9. Image Analysis

Quantification was achieved using the public-domain analysis software ImageJ. The binary image of DAPI channel was used to count the nuclei and the IMF intensity of green and red channels was obtained with a fixed threshold for each channel in the whole image (“total”). The nuclear fields (“nucleus”) for ROS were obtained using the image subtracting tool in ImageJ. Finally, the IMF intensity of nuclear ROS per cells in different conditions was calculated in an Excel spreadsheet.

2.10. Statistical analysis

All numerical data were presented as the means and standard deviations (S.D.) unless otherwise stated. Statistical analysis was performed routinely using unpaired, two-tailed *Student’s t*-test between the two experimental groups. $p<0.05$ was considered to be statistically significant.

3. Results

3.1. Overexpression of Dsg3 suppresses dome formation in confluent MDCK cultures

We have generated stable MDCK cell lines with transduction of full-length human Dsg3 (Dsg3-FL) and three Dsg3 C-terminally truncated mutants at various stretches in the extracellular domain, namely Dsg3Δ238, Dsg3Δ458, Dsg3Δ560, along with empty vector control (Vect Ct) (Fig. 1A) (Moftah et al., 2016). Western blotting analysis indicated an overall reduction of endogenous Dsg3 in these mutant cell lines (Fig. 1B). Interestingly, we observed accelerated dome formation with high frequencies in all mutant lines, with many domes occurred within a couple of days after seeded at confluent densities (Fig. 1C). In contrast, absent domes were found in Dsg3-FL cell line with Dsg3 overexpression, even in prolonged cultures of approximately 1.5 months. Vect Ct cells showed an intermediate score of the dome formation (Fig. 1D). The presented domes in mutant cells tended to rupture when the cultures were left for a couple of weeks (arrow in Fig. 1C). Treatment of mutant cells with enzymes, such as dispase (2.4 units/ml) or trypsin/EDTA, dissociated the dome cells much quicker than neighboring cells in the monolayers, suggesting their sensitivity to the enzymes that induce cell detachment from one another and/or from the substrate (Fig. 1E). This result agrees with an earlier report that the dome formation in epithelial monolayers is likely caused by a weak attachment to the substratum (Sugahara et al., 1984).

To evaluate the ageing status in MDCK cell lines, we performed staining for beta-galactosidase (β-gal), a senescence marker (β-Galactosidase Staining Kit Cat #K802-250, BioVision), and found positive staining exclusively in the dome cells (Fig. 1C) indicating the aged/differentiated phenotype as reported in the literature (Kennedy and Lever, 1984,Leighton et al., 1970,Oberleithner et al., 1990). The β-gal staining was also performed in newly re-plated cells after prolonged cultures in three cell lines (>1 month) (Fig. 2A) and again, a marked increase in β-gal positive cells was detected in the mutant populations, with a characteristic enlarged, flattening senescent cell morphology. In sharp contrast, Dsg3-FL cells presented a young, fresh appearance, with a significant decrease in β-gal staining ($p<0.001$, Fig. 2A). Collectively, these findings suggest that overexpression of Dsg3 in MDCK cells suppresses cell differentiation and ageing as indicated by absent domes and negative β-gal staining. In contrast, Dsg3ΔC mutant expression reverses this phenotype and elicits augmented cell ageing/differentiation with a concomitant high frequency of doming.

3.2. Overexpression of Dsg3 suppresses apoptosis and ROS production

We next analyzed apoptosis in aged cultures of three MDCK cell lines for Annexin V staining by FACS and observed an increased number of dead cells in Dsg3Δ458 mutant as opposed to Vect Ct and FL cells (13.78 *vs* 1.05 and 1.13, respectively, Fig 2B). The enhanced apoptosis in mutant cells was supported by DAPI staining that showed numerous DNA fragments in the dome areas (see data below). In addition, there was a ~15% reduction in live cells in Dsg3Δ458 compared to Vect Ct. Next, cell cycle analysis was performed and consistently, increased events in sub-G1 were shown in Dsg3Δ458 cell population compared to Vect Ct and FL line (14.2% *vs* 0.51% and 0.47%, respectively, Fig.2C). Interestingly, decreased events in G2/M phase and increased events in G1 phase were detected in Dsg3-FL cells relative to Vect Ct sample (G2/M: 9.29% *vs* 22.1% and G1: 75.9% *vs* 45.1% Fig. 2C), indicating the more quiescent nature than control. Furthermore, immunostaining for cleaved (active) caspase-3 revealed a

remarkable increase of caspase-3 positive cells in mutant cells compared with Vect Ct and FL cells, confirming pronounced apoptosis occurred in this population (>5-fold, **p<0.01, Fig. 2D).

Activation of ROS is crucial to trigger cell differentiation, survival, and apoptosis Coso et al., 2012; Storz, 2011). To test the relationship between ROS production and dome formation in MDCK cell lines, nuclear ROS was measured using the CellROX Oxidative Stress (Green) Reagent (Materials and Methods) which offers the advantage of determining nuclear ROS levels by fluorescence microscopy. Cells were seeded on coverslips at low and high densities for overnight before being treated with CellROX Green Reagent at a concentration of 5 µM for 30 minutes prior to fixation and immunostaining for Dsg3 using the mouse monoclonal antibody that binds to the N-terminal domain. Fluorescence microscopy showed a significant reduction of Dsg3 membrane staining in both mutant cell lines examined, compared to Vect Ct, indicating disruption of cell-cell junctions in mutant cells. In contrast, a marked increase in surface Dsg3 was shown in Dsg3-FL cells, as anticipated (Fig. 3A). Nuclear ROS indicated a significant increase in high cell densities except for Dsg3-FL that remained low at the levels comparable to low densities ($p>0.05$ Fig. 3A,B). Importantly, a marked increase of nuclear ROS was detected in both mutant lines, compared to Vect Ct, at high cell density (Fig. 3B) suggesting such elevated ROS may be attributed to cell apoptosis and premature ageing of mutants. Treatment of cells with the antioxidant α-phenyl-*N*-*tert*-butyl nitrone (PBN, 400 µM) resulted in a significant reduction of ROS (>2-fold, $p<0.05$ Fig. 3C) confirming the specificity of increased ROS caused by the oxidative stress. Next, we asked whether antioxidant treatment could diminish the domes in MDCK cells and in this case, the domed cell populations were treated with antioxidants, PBN (800 µM), N-Acetylcysteine (NAC, 2 mM), and glutathione (GSH, 10 µM) for 6 hours. Reduced dome disappearance was shown in Vect Ct cells but to a lesser degree in mutant cell lines (Fig. 3D, data not shown) suggesting other factors, in addition to ROS, may also contribute to dome formation in mutants.

Taken together, these data suggest clearly that overexpression of Dsg3 suppresses ROS production and apoptosis that limit dome formation in MDCK cells. In contrast, the expression of dominant-negative Dsg3ΔC constructs results in an inverse phenotype with enhanced oxidative stress-induced apoptosis and premature cell ageing or dome formation.

3.3. Overexpression of Dsg3 enhances TER and transepithelial permeability

To analyze the impact of ectopic Dsg3 overexpression on the functional aspect of TJs, we grew Vect Ct, Dsg3-FL and Dsg3Δ458 cell lines at confluent cell densities on Transwell filters. First, the TJ development was monitored by measuring transepithelial electrical resistance (TER) (with a Millicell ERS-2, Millipore, USA), a reliable indicator of TJ barrier function, once each day for up to 7 days (Fig. 4A). The control cells showed TER reached approximately 130 $\Omega \cdot cm^2$ at day 1, a value reported for MDCK II cells (Dukes et al., 2011,Rothen-Rutishauser et al., 1998) and then gradually increased to ~250 $\Omega \cdot cm^2$ at day 7. In striking contrast, MDCK-FL cells reached 240 $\Omega \cdot cm^2$ at day 1 and with a further increase to 500~550 $\Omega \cdot cm^2$ (>5-fold) at day 2-3 before declining to 300 $\Omega \cdot cm^2$ at day 4 and remaining at relatively higher levels than Vect Ct cells (Fig. 4A). Mutant cells, however, also displayed a slight increase with ~300 $\Omega \cdot cm^2$, but

remained significantly lower than Dsg3-FL cells ($p<0.01$, Fig. 4A). This result indicates that overexpression of Dsg3 elicits a phenotype of enhanced 'tight' junctions in MDCK cells and that Dsg3ΔC expression largely eliminated this effect, resulting in a 'leaky' junctional phenotype similar to control cells (Dukes et al., 2011). In support of this, phase contrast microscopy detected many domes in both Vect Ct and Dsg3Δ458 cell lines, but none at all in Dsg3-FL cells, grown on filters (Fig. 4C), a finding that was consistent with our earlier observations in cultures grown on the plastic substrate (Fig.1). Next, the transepithelial permeability of MDCK cell lines to a 70kDa FITC-dextran tracer was measured at various time points for up to 14 days (Fig. 4B). Unexpectedly, the results showed a 3-4-fold increase in Dsg3-FL cells after 3 days of confluent culture, compared to Vect Ct and two mutant cell lines. This was followed by a decline in the next few days but with the level still doubled that of control cells by 14 days, the end of the experiment (Fig. 4B). A slight increase for FITC-dextran flux was detected initially in mutant cell lines but this was followed by a gradual decline to the levels below control cells at the later two time points ($p<0.01$, Fig. 4B). These results suggest that overexpression of Dsg3-FL promotes transepithelial permeability, an effect being abrogated by Dsg3ΔC mutant expression.

Next, Western blotting and immunostaining analyses for ZO-1 was performed in confluent cultures grown on filters for 5 days. A reduction of ZO-1 was detected in Dsg3-FL with a moderate increase in Dsg3Δ458 compared to control (Fig. 4D). In addition, double bands were displayed in Dsg3Δ458 line. Protein distribution of ZO-1 indicated a characteristic linear TJ staining in control but with pronounced reduced intensity in Dsg3-FL cells (Fig. 5B) that also displayed a much smaller size than the other two cell lines. Intriguingly, numerous intercellular splits/cracks were observed in mutant cells with clear strong membrane staining (arrowheads Fig. 4E) suggesting an altered TJ structure.

A previous study shows that disruption of actin–myosin interaction is responsible for the increased transport activity and dome formation (Castillo et al., 2002). Therefore, we performed fluorescent staining for F-actin and Myosin IIa in confluent monolayers grown on filters (5 days). Confocal image projection showed augmentation for both cytoskeletal proteins with strong cortical ring and also strong Myosin stress fibers in mutants, and these features were drastically attenuated in Dsg3-FL cells, especially in Myosin IIa staining, relative to control cells (Fig. 5A). Confocal microscopy was also conducted in freshly seeded cells on coverslips (1 day) double-labeled for F-actin and ZO-1 (Fig. 5B,C). The XZ projection images revealed ZO-1 to be more restricted to the apical region (polarization) in Dsg3-FL compared to Vect Ct cells (relative to DAPI staining, Fig. 5B). In contrast, a marked disruption of ZO-1 with diffuse distribution was shown in the basal membrane in Dsg3Δ458 cells. Moreover, examination in the apical and basal planes within image stacks of Dsg3Δ458 cells uncovered enhanced, widespread accumulation of ZO-1 at the basal plane with only a few cells displaying linear periphery staining apically (Fig. 5C). These changes were accompanied by massive stress fibers/bundles of F-actin and less cortical actin ring in the mutant. On the other hand, Dsg3-FL cells showed predominantly peripheral ZO-1 with concomitant strong cortical F-actin accumulation at the basolateral level in contrast to Vect Ct cells, implying a hastened junction formation. Collectively, these results suggest that overexpression of Dsg3 augments TJ formation and maturation with Dsg3ΔC expression reversing this phenotype, leading to actin disorganization and/or stabilization that could be one of the causative factors underlying

accelerated doming in the mutant populations (Gourlay and Ayscough, 2005,Amberg et al., 2012). Furthermore, these findings also suggest that overexpression of Dsg3 facilitates TJ assembly and structural integrity, with enhanced TER and transepithelial permeability, which in turn limits dome forming in MDCK cells.

To confirm that actin disorganization and accumulation is also a contributing factor to the enhanced dome formation in mutant lines, we treated the domed Dsg3Δ458 cell population with the inhibitor for actin polymerization, cytochalasin B (20 μM), as well as other chemical inhibitors, including cycloheximide (3 μg/ml) (for protein synthesis), nocodazole (10 μM) (for microtubule), Rac1 inhibitor NSC23766 (30 μM) (Rac1-GEF interaction) and ROCK inhibitor Y-27632 (10 μM) (Rho-associated coiled-coil forming protein serine/threonine kinase), respectively, for one day before dome scoring. The results indicated that only cycloheximide and cytochalasin B, which inhibit protein synthesis and formation of contractile microfilaments, respectively, were able to abolish domes compared to control sample ($p<0.001$, Fig. 6) (Lever, 1979a,Lever, 1979b). Other drugs showed no statistically significant differences relative to control. Therefore, it was concluded that actin accumulation and stabilization are also responsible, at least in part, for accelerated doming in Dsg3ΔC mutants. Furthermore, the vastly disorganized F-actin may also underlie the augmented ROS levels as well as defects in TJ formation and cell to substrate attachment (Gourlay and Ayscough, 2005).

3.4 Overexpression of Dsg3 reduces cell size, while its Dsg3ΔC mutant expression promotes cell proliferation

As a smaller cell size was observed in Dsg3-FL cells, we examined the cell proliferation markers, such as Ki67 staining and Western blotting for cell cycle regulators such as Cyclin A and PCNA in confluent cultures of MDCK cell lines grown on filters (Fig. 7). Significantly, a marked increase of nuclear Ki67 was detected in Dsg3Δ458 mutant cells in contrast to Vect Ct and Dsg3-FL cell lines (Fig. 7A), suggesting elevated cell proliferation. Cell number scoring indicated an increase in Dsg3-FL (>1/3-fold) and to a lesser extent in Dsg3Δ458 cells compared to control (Fig. 7B). The increased cell number in mutants may partly reflect some damaged apoptotic cells in the populations (DAPI staining, Fig. 7A). In line with this finding, elevated expression of Cyclin A was detected in both Dsg3-FL and Dsg3Δ458 cell lines, albeit little change were shown in PCNA (Fig. 7C). Taking into account of small cell size (Fig. 4E, Fig. 7) and fresh young looking cultures as well as the quiescent feature (Fig. 2) of Dsg3-FL cells, it was concluded that overexpression of Dsg3 in MDCK cells may render a population of healthy cells with active TJ functions and suppressed ROS levels and apoptosis, resulting in an inhibition of doming. In contrast, expression of dominant-negative Dsg3ΔC in MDCK induced elevated ROS production and apoptosis as well as cell proliferation, that were likely resulted from defects in TJs accompanied with marked structural disorganization of the cytoskeleton, leading to accelerated doming (Cuevas et al., 2015,Hagen, 2017).

4. Discussion

In this study, we provide the first evidence that the desmosomal cadherin Dsg3 acts as a pro-survival protein, playing a role in maintaining cellular longevity by suppressing ROS production, apoptosis and cell differentiation as indicated by the inhibition of domes in MDCK cells. This conclusion is further supported by the observed phenotype of Dsg3ΔC mutant cells that exhibit premature doming, elevated ROS levels, and apoptosis with defects in TJs and the actin cytoskeleton. The summary of the phenotypes for Dsg3-FL and Dsg3ΔC mutant cell lines are shown in Table 1.

The paramount role of epithelial barrier function in homeostasis has long been recognized and an age-dependent change in epithelial permeability is associated with diseases in multiple organs including kidney (Parrish, 2017). A key feature of epithelial barriers is the intercellular adhesion complexes including TJs that confer both the 'fence' (maintain polarized distribution of membrane proteins and lipids) and the 'gate' (block the paracellular movement of solutes) functions. Two parameters of TJ permeability, *i.e.* TER and transepithelial solute permeability, have generally been considered to characterize the barrier function of TJs. TER is a measurement of impedance to the flow of small inorganic ions across the epithelial monolayers, whereas Transwell assay is to determine the transcellular permeability to solute (e.g. FITC-dextran). It is generally accepted that TER is associated with the quality of cultured epithelial cells, with high TER corresponding to the strength of cellular junctions, the apical–basal polarization and good healthy cultures with a sub-differentiated cell status (Chen et al., 2015). In this study, both parameters were assessed in our generated MDCK cell lines with transduction of Dsg3-FL or its C-terminally truncated Dsg3ΔC mutants and the results showed that Dsg3 is capable of regulating the TJ barrier function in MDCK cells with its overexpression rendering a marked transient increase of TER (>500 Ω·cm2) as well as, intriguingly, the transepithelial flux of FITC-dextran (discussed below), with peaks at 2-3 days (Fig. 4A,B). Although a decline in both parameters was observed after 3 days, the levels remained significantly higher than control cells as well as mutants. These results may suggest more active TJ functions operating in Dsg3-FL cells that enable the maintenance of large gradients for electrolytes.

Changes in TER is determined by the different molecular composition and subcellular distribution of TJ proteins. Indeed, immunoflurescence and Western blotting analyses in the well established confluent cultures grown on filters revealed restricted protein expression and distribution of ZO-1 in Dsg3-FL cell line but strong membrane staining with marked splits or cracks present in Dsg3Δ458 mutant (Fig. 4D,E), indicating the disruption of TJ integrity. In support, fluorescent staining for F-actin and Myosin IIa detected the marked accumulation of both cytoskeletal proteins as well as numerous Myosin IIa stress fibers in mutant cells, but a pronounced attenuation was shown in Dsg3-FL cells, especially for Myosin IIa staining (Fig. 5A). The disruption of actin in mutant was also observed in freshly seeded cells on coverslips with massive accumulation of F-actin bundles coupled with ZO-1 internalization at the basal level of mutant cells (Fig.5B,C). In sharp contrast, strong cortical F-actin rings coupled with linear peripheral ZO-1 staining was evident in FL cell line with reduced intensity in control cells (Fig. 5C). These results collectively suggest that overexpression of Dsg3 in MDCK cells facilitates TJ formation and integrity that may contribute to heightened TER observed in this cell line. On the other hand, changes in ZO-1 and cytoskeleton coupled with elevated ROS and apoptosis in Dsg3ΔC mutant may imply a prematurely aged phenotype. Overall, our study suggests that the cytoplasmic domain of Dsg3 is essential for the proper function of TJs since

expression of Dsg3ΔC truncated mutants failed to induce heightened TER as Dsg3-FL cells did but rather had the TER values close to Vect control cells (Fig. 4A) with relatively 'leaky' TJ property (MDCK II). Hence, it is possible that cytoplasmic tail of Dsg3 interacts and/or recruits TJ proteins to the plasma membrane to facilitate the junction formation as shown in ZO-1 and F-actin staining in this study as well as reported previously (Brown et al., 2014,Tsang et al., 2010,Tsang et al., 2012b,Tsang et al., 2012a).

The actin and nonmuscle actomyosin can have a major impact on cell fate and well-being and is crucial in controlling many cellular processes, such as the generation and maintenance of cell junctions, high TER, cell shape, polarity, motility as well as intracellular trafficking (Gourlay and Ayscough, 2005,Castillo et al., 2002). Inhibition of myosin ATPase induces dome formation coupled with decreased TER in MDCK monolayers (Castillo et al., 2002). Central to the proper function of actin is its dynamic structure. Increased F-actin turnover can promote cell longevity and decrease ROS production. On the other hand, decreased actin turnover can trigger cell death through increased levels of ROS and apoptosis-like pathway (Gourlay and Ayscough, 2005). Our previous studies show that overexpression of Dsg3 in MDCK cells enhances actin dynamics and turnover as well as E-cadherin trafficking (Tsang et al., 2012a,Moftah et al., 2016). Here in this present study, we provide further evidence that overexpression of Dsg3 in MDCK cells boosts cell well-being by suppressing ROS levels, apoptosis, and doming with enhanced TJ structural and functional integrity. Collectively, these results suggest strongly that Dsg3 may act as an anti-ageing protein and help maintain cellular health and longevity. This conclusion was further supported by the observation of an inverse phenotype in Dsg3ΔC mutants (Fig. 2) with defects in TJs and structural rearrangement of the cytoskeleton (Fig. 4, Fig. 5). The accumulation of ROS also has a detrimental effect on cell well-being and is associated with apoptosis and ageing. This was supported by the findings that either antioxidant treatment or inhibition of F-actin network (cytochalasin B) as well as protein synthesis (cycloheximide) can abolish dome formation in control and mutant cell lines, respectively (Fig. 3D, Fig. 7). It has been shown that in both yeast and mammalian systems, changes to the dynamics and stabilization of actin lead to the release of ROS from mitochondria and subsequent cell death (Gourlay and Ayscough, 2005). Therefore, the elevated ROS in Dsg3ΔC mutants could be caused by a defect in the actin cytoskeleton in these cells.

Some discrepancies between structural and functional data were observed in this study. For instance, Dsg3-FL cells exhibited an increased TER as well as augmented FITC-dextran flux (Fig. 4B) suggesting uncoupling of TER and paracellular permeability in this cell line. In Dsg3ΔC mutant cells, alterations in the TJ structure failed to correlate well with the functional data that showed moderately enhanced TJ barrier function relative to control cell line (Fig. 4A,B). However, discrepancies between the barrier permeability and apical cell junctions have been reported (Beeman et al., 2009,Petit et al., 2003). In addition, uncoupling between TER and macromolecule permeability has been demonstrated in a recent study (Otani et al., 2019). Although the molecular mechanisms for the phenotypes in our generated MDCK cell lines remain elusive, it was thought that multiple factors may be involved in these alterations (Table 1). First, changes in TJ protein composition and distribution could be a contributing factor. Here only ZO-1 and F-actin and Myosin IIa were analyzed. There are many proteins existing in TJs, including claudins, occludin, and JAMs (Balkovetz, 2009). It has been shown that the coordinated operation of claudins and JAM-A is responsible for the TJ permeability barrier to macromolecules (Otani et al., 2019). On the other hand, claudins are regarded as

the sealing proteins responsible for the TJ barrier function to ions and solutes in MDCK cells (Furuse et al., 2001). Thus, it could well be that some alterations in TJ protein complex including claudins and JAM-A occur in Dsg3-FL cells which warrants further investigation. Alternatively, these changes might simply reflect a young healthy cellular property with reduced ROS and apoptosis as shown in FL cells (Fig. 1-3). In line with this notion, we also uncover that Dsg3 exerts a function in the suppression of p53 (Rehman et al., 2019). Furthermore, marked suppression of phospho-YAP, an indicator of Hippo that controls cell differentiation was also observed in Dsg3-FL in contrast to Vect control and Dsg3ΔC cell lines (our unpublished data). On the other hand, the moderately increased transepithelial permeability shown in Dsg3ΔC mutants, compared to control cells, is likely caused by enhanced cytoskeletal protein expression at the junctions. Alternatively, it was thought that this might not truly reflect an enhanced barrier but rather be due to other factors such as increased apoptosis and high frequency of large domes that cause physical obstruction of barrier permeability for dextran and electrolytes across the monolayers. In addition, we also observed that mutant cells were taller than FL and control cell lines (~30% higher) that may result in a delay of transepithelial solute flux.

Unexpectedly, a large increase of nuclear Ki67 staining, as well as elevated Cyclin A, was found in Dsg3Δ458 cells compared to control cells (Fig. 7B,C). Such elevated cell proliferation may partly contribute to accelerated doming in the mutant populations since it was shown that antioxidant treatment was unable to abrogate the domes effectively. In addition, this may reflect the nature of exaggerated replacement for the loss of apoptotic cells in these populations. Interestingly, the young cell trait with fresh-looking, small cell morphology coupled with increased cell counting, as well as the quiescent feature was observed in FL cell line compared to other cell lines (Fig. 2C, Fig. 4E, Fig. 7). It is considered that, unlike skin and liver in which the baseline cell turnover is fast, the healthy kidney is a relatively stable organ with little baseline cell turnover (Castrop, 2019). Thus, the findings of the quiescent nature of Dsg3-FL cells may indicate a stable healthy culture status as described above. In summary, this study uncovers a novel role for Dsg3, beyond the regulation of desmosome adhesion, in the maintenance of cell well-being and inhibition of ROS production, apoptosis and dome formation. In support, the expression of Dsg3ΔC mutant in MDCK cells elicits an inverse phenotype with elevated ROS, apoptosis and premature doming that were likely resulting from defects in TJs and the cytoskeleton structural organization.

Author Contributions

XI, USA, YYH, JU, AR, GW, and HW conceived and performed the experiments and analyzed the data. EKP and SM assisted with some experiments including the antioxidant treatment and TJ functional assays. HW and EKP wrote the manuscript, and SM edited the manuscript.
This work was partially supported by a scholarship from Naresuan University, Phitsanulok, Thailand. All authors reviewed and proofread the manuscript. HW takes full responsibility for the contents of the publication.

References

Amagai, M., Klaus-Kovtun,V., Stanley,J.R., 1991. Autoantibodies against a novel epithelial cadherin in pemphigus vulgaris, a disease of cell adhesion. Cell. 67(5), 869-877.

Amberg, D., Leadsham,J.E., Kotiadis,V., Gourlay,C.W., 2012. Cellular ageing and the actin cytoskeleton. Subcell Biochem. 57, 331-352.

Balkovetz, D.F., 2009. Tight junction claudins and the kidney in sickness and in health. Biochim Biophys Acta. 1788(4), 858-863.

Beeman, N.E., Baumgartner,H.K., Webb,P.G., Schaack,J.B., Neville,M.C., 2009. Disruption of occludin function in polarized epithelial cells activates the extrinsic pathway of apoptosis leading to cell extrusion without loss of transepithelial resistance. BMC Cell Biol. 10, 85.

Brown, L., Wan,H., 2015. Desmoglein 3: a help or a hindrance in cancer progression? Cancers (Basel). 7(1), 266-286.

Brown, L., Waseem,A., Cruz,I.N., Szary,J., Gunic,E., Mannan,T., Unadkat,M., Yang,M., Valderrama,F., O'Toole,E.A., Wan,H., 2014. Desmoglein 3 promotes cancer cell migration and invasion by regulating activator protein 1 and protein kinase C-dependent-Ezrin activation. Oncogene. 33(18), 2363-2374.

Castillo, A.M., Reyes,J.L., Sanchez,E., Mondragon,R., Meza,I., 2002. 2,3-butanedione monoxime (BDM), a potent inhibitor of actin-myosin interaction, induces ion and fluid transport in MDCK monolayers. J Muscle Res Cell Motil. 23(3), 223-234.

Castrop, H., 2019. The Role of Renal Interstitial Cells in Proximal Tubular Regeneration. Nephron. 141(4), 265-272.

Chen, S., Einspanier,R., Schoen,J., 2015. Transepithelial electrical resistance (TEER): a functional parameter to monitor the quality of oviduct epithelial cells cultured on filter supports. Histochem Cell Biol. 144(5), 509-515.

Coresh, J., Byrd-Holt,D., Astor,B.C., Briggs,J.P., Eggers,P.W., Lacher,D.A., Hostetter,T.H., 2005. Chronic kidney disease awareness, prevalence, and trends among U.S. adults, 1999 to 2000. J Am Soc Nephrol. 16(1), 180-188.

Cristante, E., McArthur,S., Mauro,C., Maggioli,E., Romero,I.A., Wylezinska-Arridge,M., Couraud,P.O., Lopez-Tremoleda,J., Christian,H.C., Weksler,B.B., Malaspina,A., Solito,E., 2013. Identification of an essential endogenous regulator of blood-brain barrier integrity, and its pathological and therapeutic implications. Proc Natl Acad Sci U S A. 110(3), 832-841.

Cuevas, M.E., Gaska,J.M., Gist,A.C., King,J.M., Sheller,R.A., Todd,M.C., 2015. Estrogen-dependent expression and subcellular localization of the tight junction protein claudin-4 in HEC-1A endometrial cancer cells. Int J Oncol. 47(2), 650-656.

Dukes, J.D., Whitley,P., Chalmers,A.D., 2011. The MDCK variety pack: choosing the right strain. BMC Cell Biol. 12, 43.

Furuse, M., Furuse,K., Sasaki,H., Tsukita,S., 2001. Conversion of zonulae occludentes from tight to leaky strand type by introducing claudin-2 into Madin-Darby canine kidney I cells. J Cell Biol. 153(2), 263-272.

Gourlay, C.W., Ayscough,K.R., 2005. The actin cytoskeleton: a key regulator of apoptosis and ageing? Nat Rev Mol Cell Biol. 6(7), 583-589.

Grams, M.E., Chow,E.K., Segev,D.L., Coresh,J., 2013. Lifetime incidence of CKD stages 3-5 in the United States. Am J Kidney Dis. 62(2), 245-252.

Haddad, M., Lin,F., Dwarakanath,V., Cordes,K., Baum,M., 2005. Developmental changes in proximal tubule tight junction proteins. Pediatr Res. 57(3), 453-457.

Hagen, S.J., 2017. Non-canonical functions of claudin proteins: Beyond the regulation of cell-cell adhesions. Tissue Barriers. 5(2), e1327839.

Joseph, J.A., Cao,G., Cutler,R.C., 1995. In vivo or in vitro administration of the nitrone spin-trapping compound, n-tert-butyl-alpha-phenylnitrone, (PBN) reduces age-related deficits in striatal muscarinic receptor sensitivity. Brain Res. 671(1), 73-77.

Kennedy, B.G., Lever,J.E., 1984. Regulation of Na+,K+-ATPase activity in MDCK kidney epithelial cell cultures: role of growth state, cyclic AMP, and chemical inducers of dome formation and differentiation. J Cell Physiol. 121(1), 51-63.

Leighton, J., Estes,L.W., Mansukhani,S., Brada,Z., 1970. A cell line derived from normal dog kidney (MDCK) exhibiting qualities of papillary adenocarcinoma and of renal tubular epithelium. Cancer. 26(5), 1022-1028.

Lever, J.E., 1979a. Inducers of mammalian cell differentiation stimulate dome formation in a differentiated kidney epithelial cell line (MDCK). Proc Natl Acad Sci U S A. 76(3), 1323-1327.

Lever, J.E., 1979b. Regulation of dome formation in differentiated epithelial cell cultures. J Supramol Struct. 12(2), 259-272.

Moftah, H., Dias,K., Apu,E.H., Liu,L., Uttagomol,J., Bergmeier,L., Kermorgant,S., Wan,H., 2016. Desmoglein 3 regulates membrane trafficking of cadherins, an implication in cell-cell adhesion. Cell Adh Migr., 1-22.

Oberleithner, H., Vogel,U., Kersting,U., 1990. Madin-Darby canine kidney cells. I. Aldosterone-induced domes and their evaluation as a model system. Pflugers Arch. 416(5), 526-532.

Otani, T., Nguyen,T.P., Tokuda,S., Sugihara,K., Sugawara,T., Furuse,K., Miura,T., Ebnet,K., Furuse,M., 2019. Claudins and JAM-A coordinately regulate tight junction formation and epithelial polarity. J Cell Biol.

Parrish, A.R., 2017. The impact of aging on epithelial barriers. Tissue Barriers. 5(4), e1343172.

Petit, L., Gibert,M., Gourch,A., Bens,M., Vandewalle,A., Popoff,M.R., 2003. Clostridium perfringens epsilon toxin rapidly decreases membrane barrier permeability of polarized MDCK cells. Cell Microbiol. 5(3), 155-164.

Reyes, J.L., Lamas,M., Martin,D., del Carmen,N.M., Islas,S., Luna,J., Tauc,M., Gonzalez-Mariscal,L., 2002. The renal segmental distribution of claudins changes with development. Kidney Int. 62(2), 476-487.

Rehman, A., Cai,Y., Hünefeld,C., Jedličková,H., Huang,Y., Teh,M.T., Ahmad,U.S., Uttagomol,J., Wang,Y., Kang,A., Warnes,G., Harwood,C., Bergamaschi,D., Parkinson,E.K., Röcken,M., Wan,H., 2019. The desmosomal cadherin desmoglein-3 acts as a keratinocyte anti-stress protein via suppression of p53. Cell Death Dis. 10(10), 750.

Rothen-Rutishauser, B., Kramer,S.D., Braun,A., Gunthert,M., Wunderli-Allenspach,H., 1998. MDCK cell cultures as an epithelial in vitro model: cytoskeleton and tight junctions as indicators for the definition of age-related stages by confocal microscopy. Pharm Res. 15(7), 964-971.

Stewart, J.H., McCredie,M.R., Williams,S.M., 2006. Geographic, ethnic, age-related and temporal variation in the incidence of end-stage renal disease in Europe, Canada and the Asia-Pacific region, 1998-2002. Nephrol Dial Transplant. 21(8), 2178-2183.

Su, H.W., Yeh,H.H., Wang,S.W., Shen,M.R., Chen,T.L., Kiela,P.R., Ghishan,F.K., Tang,M.J., 2007. Cell confluence-induced activation of signal transducer and activator of transcription-3 (Stat3) triggers epithelial dome formation via augmentation of sodium hydrogen exchanger-3 (NHE3) expression. J Biol Chem. 282(13), 9883-9894.

Sugahara, K., Caldwell,J.H., Mason,R.J., 1984. Electrical currents flow out of domes formed by cultured epithelial cells. J Cell Biol. 99(4 Pt 1), 1541-1544.

Teh, M.T., Parkinson,E.K., Thurlow,J.K., Liu,F., Fortune,F., Wan,H., 2011. A molecular study of desmosomes identifies a desmoglein isoform switch in head and neck squamous cell carcinoma. J Oral Pathol Med. 40(1), 67-76.

Tsang, S.M., Brown,L., Gadmor,H., Gammon,L., Fortune,F., Wheeler,A., Wan,H., 2012a. Desmoglein 3 acting as an upstream regulator of Rho GTPases, Rac-1/Cdc42 in the regulation of actin organisation and dynamics. Exp Cell Res. 318(18), 2269-2283.

Tsang, S.M., Brown,L., Lin,K., Liu,L., Piper,K., O'Toole,E.A., Grose,R., Hart,I.R., Garrod,D.R., Fortune,F., Wan,H., 2012b. Non-junctional human desmoglein 3 acts as an upstream regulator of Src in E-cadherin adhesion, a pathway possibly involved in the pathogenesis of pemphigus vulgaris. J Pathol. 227(1), 81-93.

Tsang, S.M., Liu,L., Teh,M.T., Wheeler,A., Grose,R., Hart,I.R., Garrod,D.R., Fortune,F., Wan,H., 2010. Desmoglein 3, via an interaction with E-cadherin, is associated with activation of Src. PLoS One. 5(12), e14211.

Figure legends

Fig. 1. Dsg3ΔC mutant expression enhances dome formation in MDCK cells. A) Schematic of Dsg3 FL and its C-terminally truncated proteins. B) Western blots for the Dsg3 expression in MDCK cell lines. C) Phase-contrast images of confluent cultures in MDCK Vect Ct, FL and Dsg3Δ456 lines with a characteristic dome shown in the mutant cells only. The arrow in one of the images below indicated dome ruptures in the mutant and the right image showed positive β-gal staining of the dome cells. D) Dome score in five MDCK stable lines (n=18) that showed a significant increase of dome scores in all three mutant lines compared with Vect Ct. In contrast, marked suppression of dome formation was showed in FL cells. (*p <0.05; ***p <0.001). E) Phase-contrast images of the dome cells treated with dispase (2.4 unit/ml) and trypsin/EDTA (0.25%), respectively. Cells in the domes appeared more readily detached from one another and also from the substrate.

Fig. 2. Enhanced apoptosis was shown in MDCK mutant cell lines. A) β-gal staining in re-plated cells after prolonged culture with quantitation shown on the right. B,C) FACS analysis of Annexin V staining and cell cycle in MDCK cell lines after prolonged culture (>1 month). D) Immunostaining with anti-cleaved caspase-3 in confluent cultures grown on Transwell filters for 5 days and the quantitation data is shown on the right. (**p<0.01, ***p<0.001, NS: no significance.) Scale bar, 10 μm.

Fig. 3. Overexpression of Dsg3 suppresses ROS and the expression of its truncated Dsg3ΔC mutant augments ROS production in cells of high density. A) Fluorescent images of Dsg3 and nuclear ROS expression in MDCK Vect Ct, FL, and Dsg3Δ458 mutant lines. Increased nuclear ROS was evident in both mutant lines compared to control and FL cells, the latter of which displayed a significant reduction. B) Quantitation of the nuclear ROS in images shown in A (n=7 in each cell line, pooled from two independent experiments). C) Inhibition of ROS by PBN, an antioxidant. Cells were treated with PBN at the final concentration of 400 μM for 1 day before ROS measurement. D) Dome scores in prolonged cultures of Vect Ct cell line before and after 6 hours treatment with antioxidants, PBN (800μM), NAC (2mM) and GSH (10μM). (*p<0.05, **p<0.01, ***p<0.001, ****p<0.0001, NS: no significance.) Scale bar, 10 μm.

Fig. 4. Overexpression of Dsg3 enhances TER and transepithelial permeability in MDCK cells grown on Transwell filters. A) TER measurement (mean ± S.D., n=6, a representative of two independent experiments). TER in Dsg3-FL cells transiently reached a maximum at day 2-3, and then settled to a lower value but remained higher than Vect control and Dsg3Δ458 lines. Such a rapid rise in FL around day 2-3 was never observed in other two cell lines although mutant also displayed an increase relative to control. B) Permeability coefficients to 70kDa FITC-dextran (mean±S.E.M.). The paracellular flux of FITC-dextran was significantly increased in Dsg3-FL cells whereas both Dsg3ΔC mutant lines showed similar patterns with a decrease at the latter two time points compared to control cells. (*p<0.05, **p<0.01, ***p<0.001, ****p<0.0001). C) Phase-contrast images of the monolayers in three cell lines grown on the filters for 10 days. Both Vect Ct and Dsg3Δ458 mutant lines showed many domes but none in FL cells. D) Western blotting for ZO-1 in lysates extracted in confluent cultures grown on filters (5 days) indicated a reduction in Dsg3-FL line compared to control as well as mutants. E) Confocal images of ZO-1 in the same confluent culture condition and the cells were fixed with formaldehyde and permeabilized with Triton for 5 minutes. Note limited ZO-1 at TJs was

shown in FL cells with morphology appearing much smaller than the other two cell lines. In contrast, numerous intercellular splits/cracks with strong membrane staining were presented in mutant cells (arrowheads). Scale bar in (C) is 100 μm and (E) is 10 μm.

Fig. 5. Confocal microscopy revealed altered cytoskeletal structures of F-actin and Myosin IIa between MDCK cell lines. A) Confocal Z projections of three cell lines, grown on filter for 5 days, labeled for F-actin and Myosin IIa, respectively. Note that a slight reduction of cortical F-actin but with significant suppression of Myosin IIa was shown in Dsg3-FL cells compared to Vect Ct and mutant lines. In contrast, a marked increase for both proteins, including the cortical F-actin bundles and Myosin stress fibers, was shown in mutant compared to controls. B) The XZ images of confocal stacks in three MDCK lines, seeded on coverslips for 1 day, labeled for ZO-1 and counterstained with DAPI for nuclei. A broad distribution of ZO-1 at the basolateral region was detected in Dsg3Δ458 mutant compared to Vect Ct and FL cells. On the other hand, Dsg3-FL cells showed more polarized, restricted apical distribution of ZO-1 with respect to DAPI nuclear staining than Vect Ct cells. C) The XY slices in apical and basal planes from confocal stacks in MDCK cell lines, seeded on coverslips (1 day), double-labeled with A488-phalloidin for F-actin and ZO-1 shown in B. Many mutant cells showed the absence of F-actin/ZO-1 at the apical plane with concomitantly massive ZO-1 accumulation and strong F-actin bundles occurred in the cytoplasm at the basal level at which FL cells still presented strong cortical F-actin and more linear ZO-1 staining compared to control cells. Scale bar, 10 μm.

Fig. 6. Dome formation was abrogated by drugs that inhibit protein synthesis and actin polymerization. A) Phase-contrast images of Dsg3Δ458 mutant cells treated with various drugs, *i.e.* cycloheximide (3 μg/ml), nocodazole (10 μM), Rac1 inhibitor NSC23766 (30 μM) and ROCK inhibitor Y-27632 (10 μM), respectively, alongside with DMSO vehicle control for 1 day. The scale bar is 100 μm. B) Dome score in the monolayers of Dsg3Δ458 mutant shown in A ($n>12$ fields per sample were scored, ***$p<0.01$). Cells were treated with drugs for 1 day before the dome scoring.

Fig. 7. Altered cell proliferation was shown in Dsg3-FL and Dsg3Δ458 cell lines. A) Ki67 and DAPI nuclear staining in three MDCK cell lines. The lower panels are the binary images of the DAPI channel that highlight increased apoptotic particles in mutant as well as Vect Ct cell line. In contrast, almost doubled nuclear number with little apoptotic particles was presented in FL cell line. A marked increased nuclear Ki67 staining displayed in mutant compared to Vect Ct and FL lines. B) Quantitation for Ki67 staining and nuclear number counting shown in A. C) Western blotting analysis for Cyclin A and PCNA, the cell cycle progression regulators. Scale bar, 10 μm.

Table 1. Summary for the phenotypes of Dsg3-FL and Dsg3ΔC cell lines.

Fig. 1

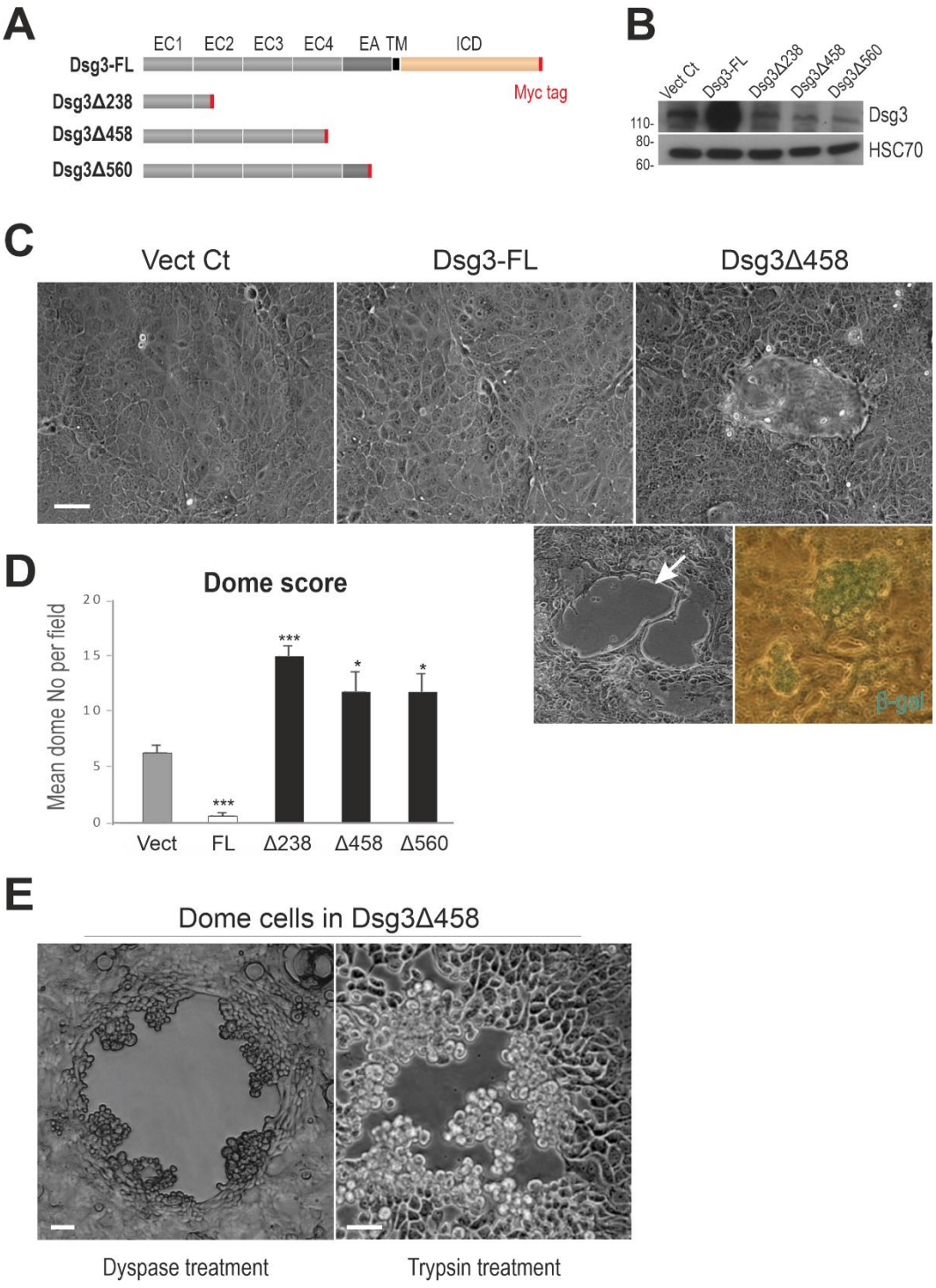
A
EC1
EC2
EC3
EC4
EA TM
ICD
Dsg3-FL
Myc tag
Dsg3Δ238
Dsg3Δ458
Dsg3Δ560
B
Vect Ct
Dsg3-FL
Dsg3Δ238
Dsg3Δ458
Dsg3Δ560
110-
80-
60-
Dsg3
HSC70
C
Vect Ct
Dsg3-FL
Dsg3Δ458
β-gal
D
Dome score
Mean dome No per field
20
15
10
5
0
***
***
*
*
Vect
FL
Δ238
Δ458
Δ560
E
Dome cells in Dsg3Δ458
Dyspase treatment
Trypsin treatment

Fig. 2

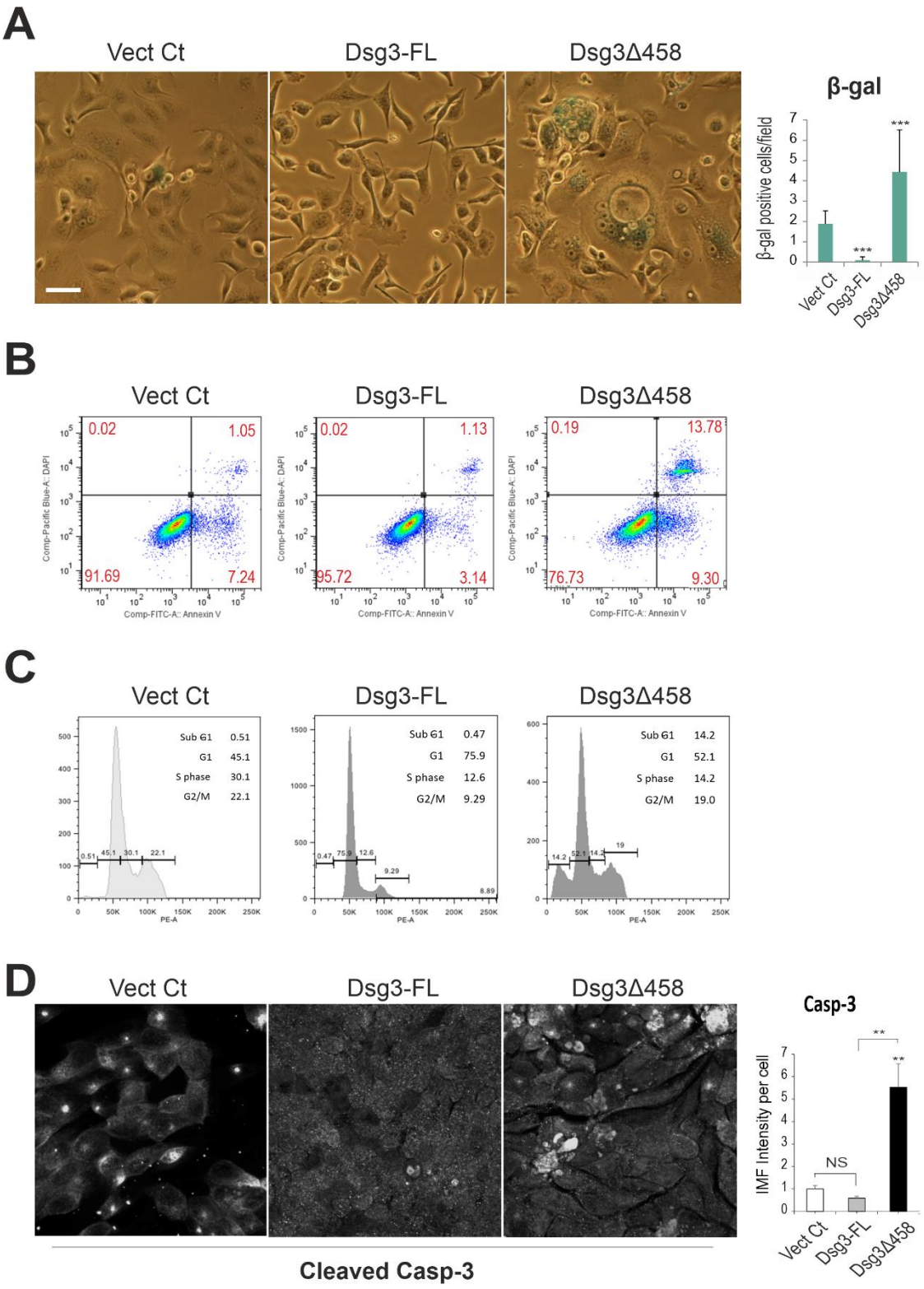
A
Vect Ct
Dsg3-FL
Dsg3Δ458
β-gal
β-gal positive cells/field
***
***
Vect Ct
Dsg3-FL
Dsg3Δ458
B
Vect Ct
Dsg3-FL
Dsg3Δ458
0.02
1.05
91.69
7.24
0.02
1.13
95.72
3.14
0.19
13.78
76.73
9.30
Comp-Pacific Blue-A:: DAPI
Comp-FITC-A:: Annexin V
C
Vect Ct
Dsg3-FL
Dsg3Δ458
Sub G1 0.51
G1 45.1
S phase 30.1
G2/M 22.1
Sub G1 0.47
G1 75.9
S phase 12.6
G2/M 9.29
Sub G1 14.2
G1 52.1
S phase 14.2
G2/M 19.0
PE-A
D
Vect Ct
Dsg3-FL
Dsg3Δ458
Casp-3
IMF Intensity per cell
NS
**
**
Vect Ct
Dsg3-FL
Dsg3Δ458
Cleaved Casp-3

Fig. 3

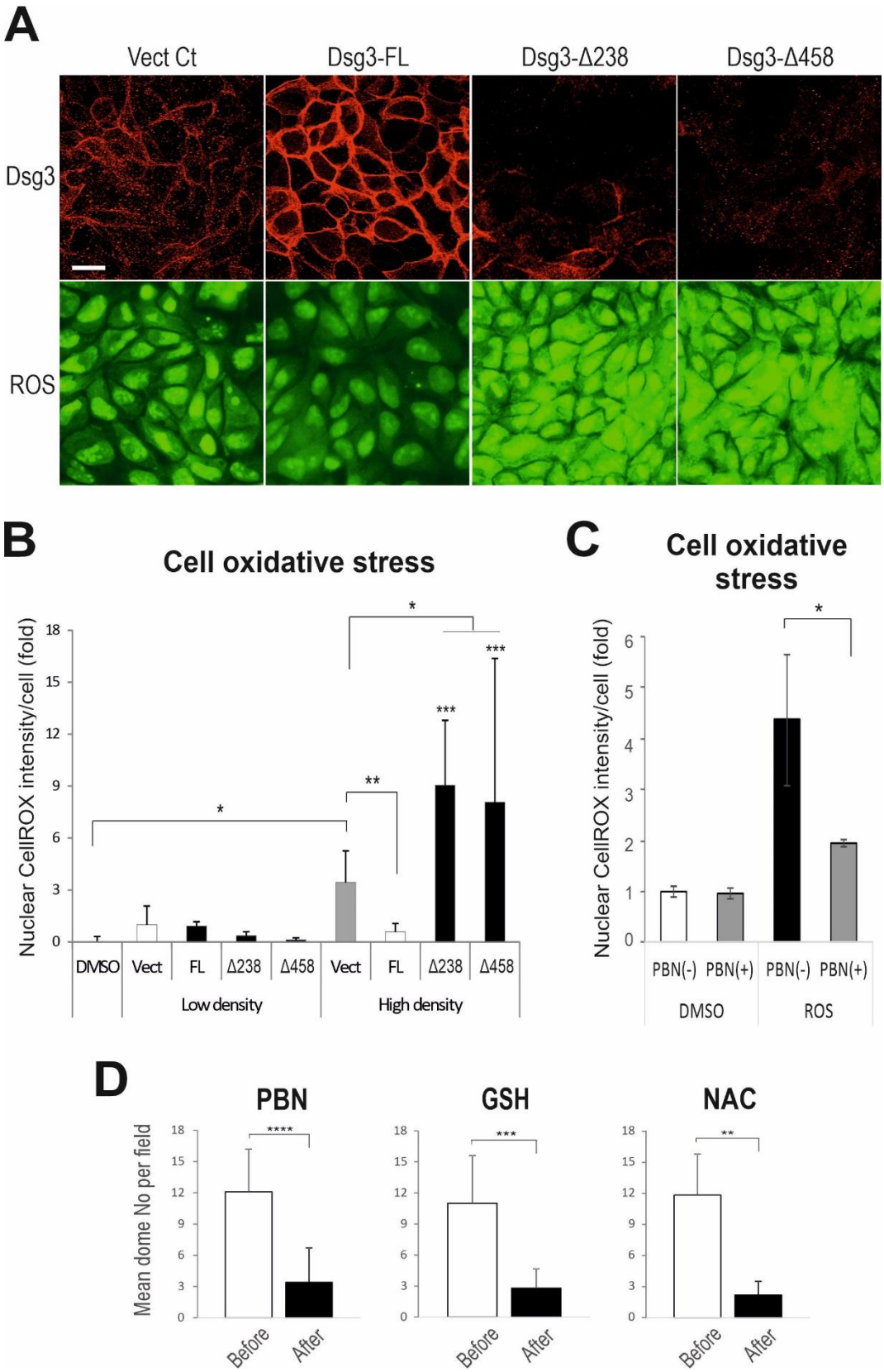
A
Vect Ct
Dsg3-FL
Dsg3-Δ238
Dsg3-Δ458
Dsg3
ROS
B
Cell oxidative stress
Nuclear CellROX intensity/cell (fold)
DMSO
Vect
FL
Δ238
Δ458
Low density
High density
C
Cell oxidative stress
PBN(-)
PBN(+)
DMSO
ROS
D
PBN
GSH
NAC
Mean dome No per field
Before
After

Fig. 4

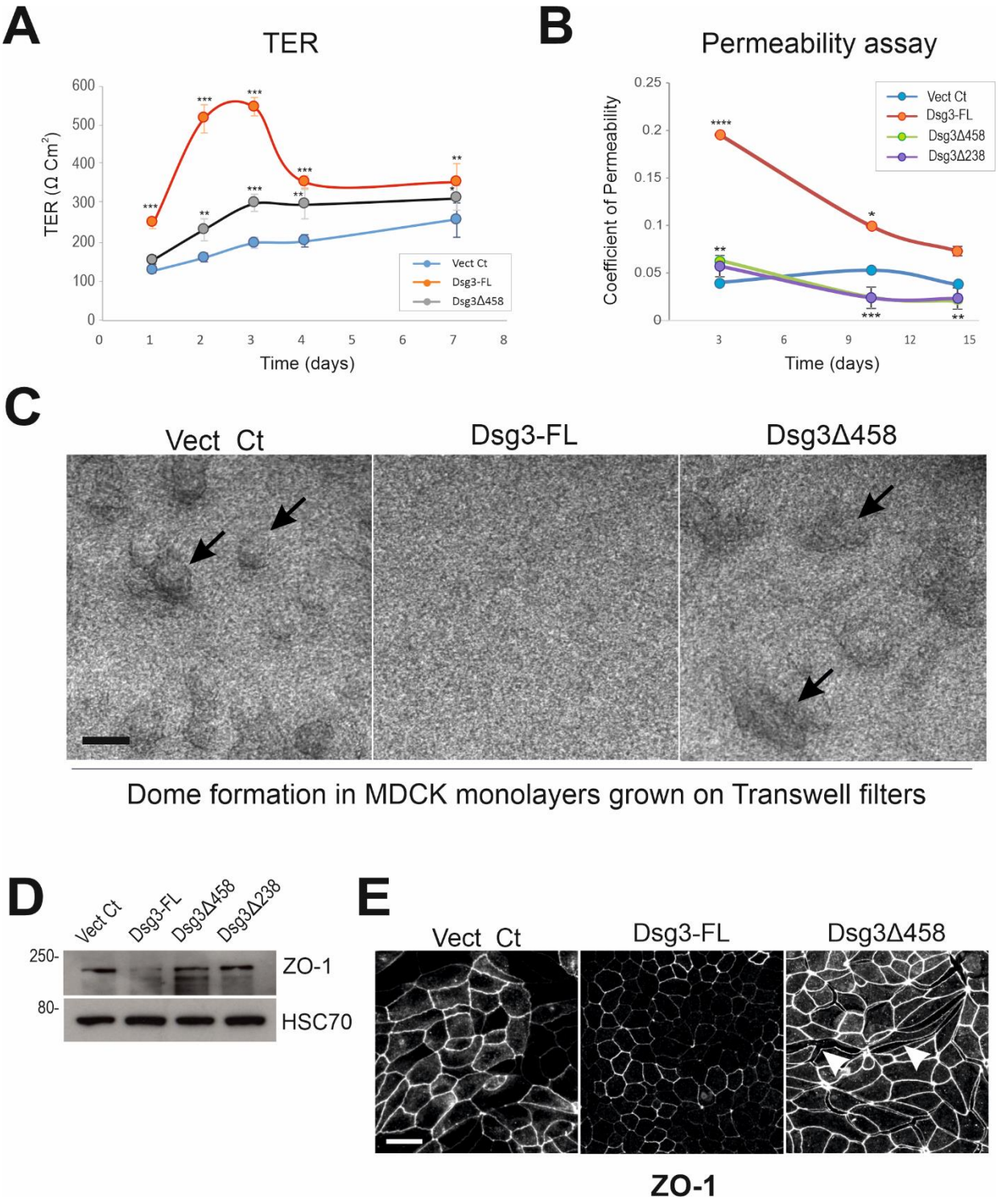
A
TER
TER (Ω Cm²)
Time (days)
Vect Ct
Dsg3-FL
Dsg3Δ458
B
Permeability assay
Coefficient of Permeability
Time (days)
Vect Ct
Dsg3-FL
Dsg3Δ458
Dsg3Δ238
C
Vect Ct
Dsg3-FL
Dsg3Δ458
Dome formation in MDCK monolayers grown on Transwell filters
D
Vect Ct
Dsg3-FL
Dsg3Δ458
Dsg3Δ238
250-
80-
ZO-1
HSC70
E
Vect Ct
Dsg3-FL
Dsg3Δ458
ZO-1

Fig. 5

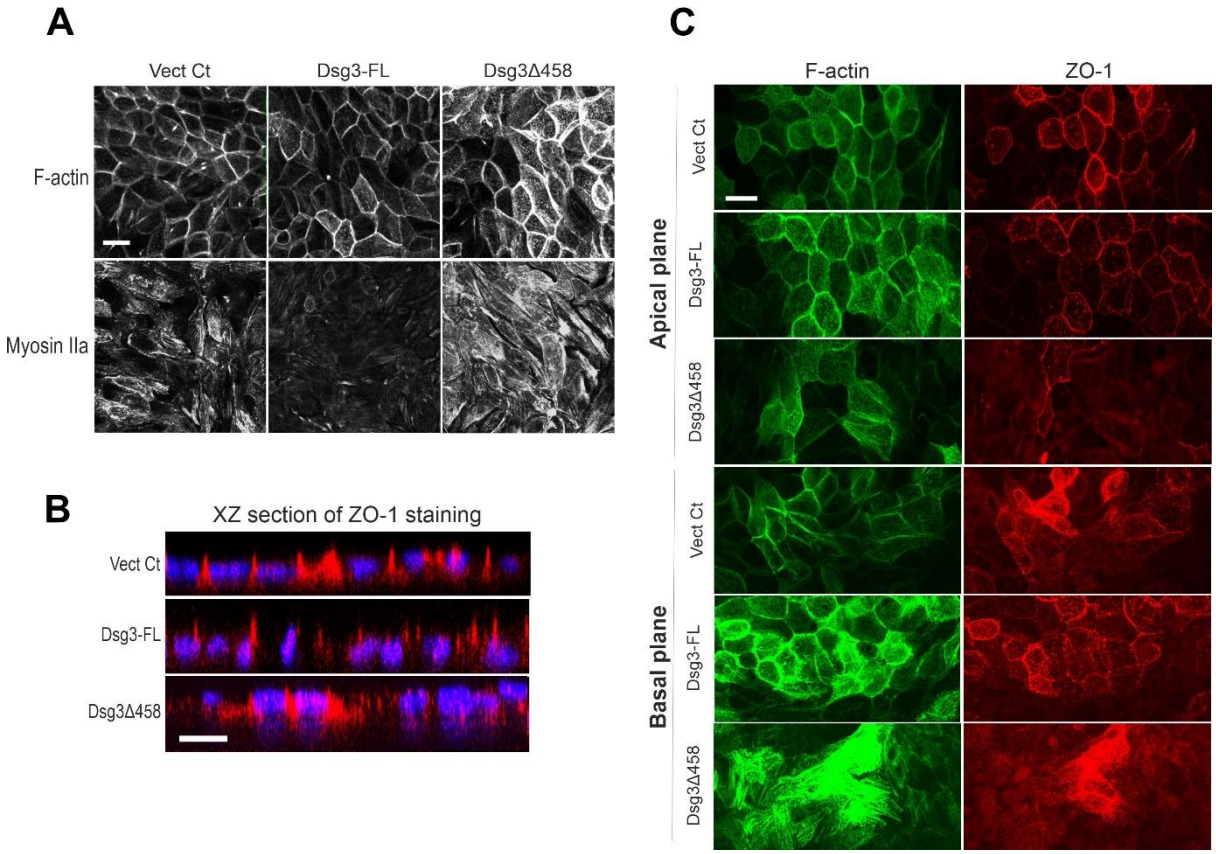
A
Vect Ct
Dsg3-FL
Dsg3Δ458
F-actin
Myosin IIa
B
XZ section of ZO-1 staining
Vect Ct
Dsg3-FL
Dsg3Δ458
C
F-actin
ZO-1
Apical plane
Basal plane
Vect Ct
Dsg3-FL
Dsg3Δ458

Fig. 6

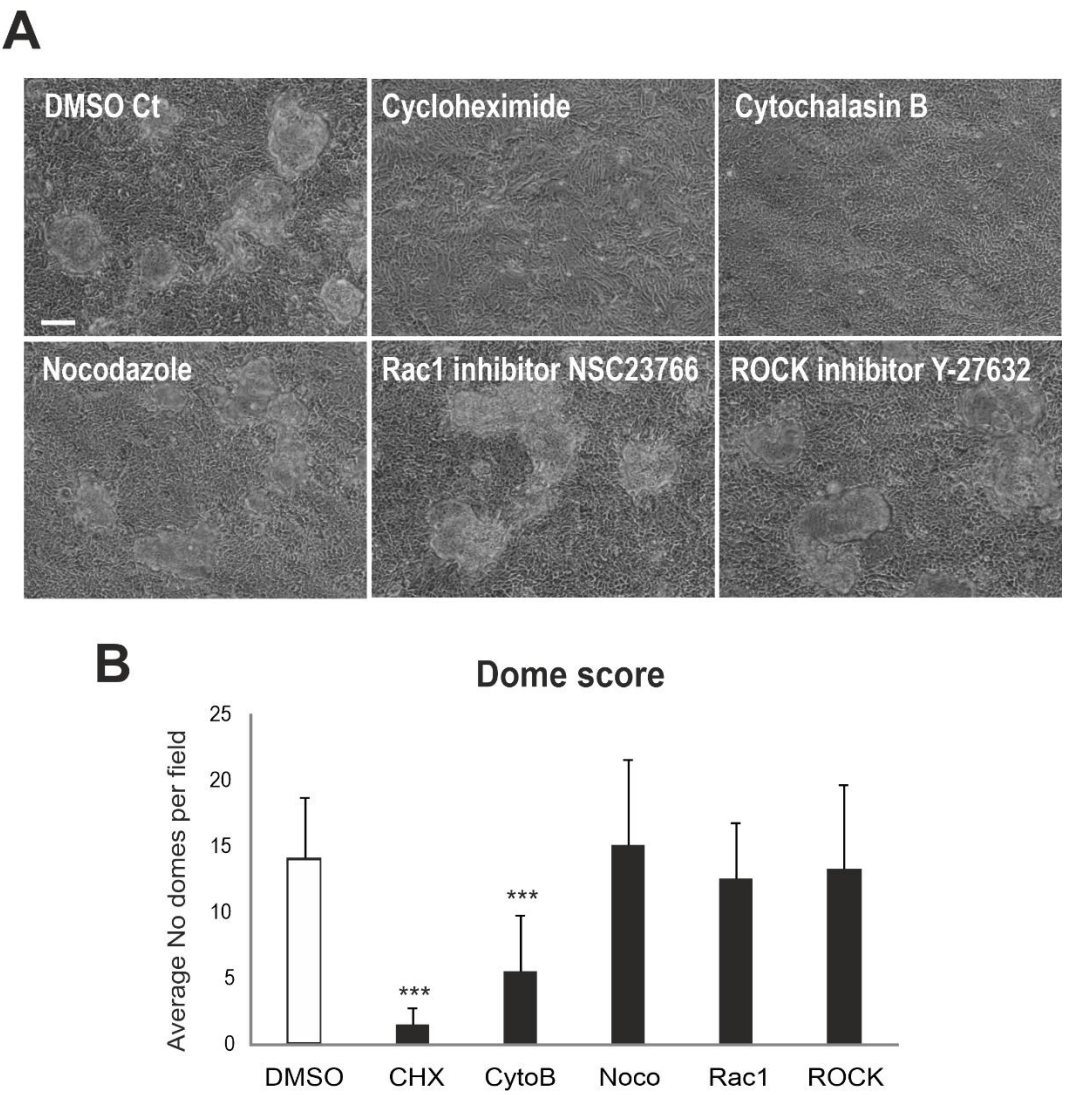
A
DMSO Ct
Cycloheximide
Cytochalasin B
Nocodazole
Rac1 inhibitor NSC23766
ROCK inhibitor Y-27632
B
Dome score
Average No domes per field
25
20
15
10
5
0
***
***
DMSO
CHX
CytoB
Noco
Rac1
ROCK

Fig. 7

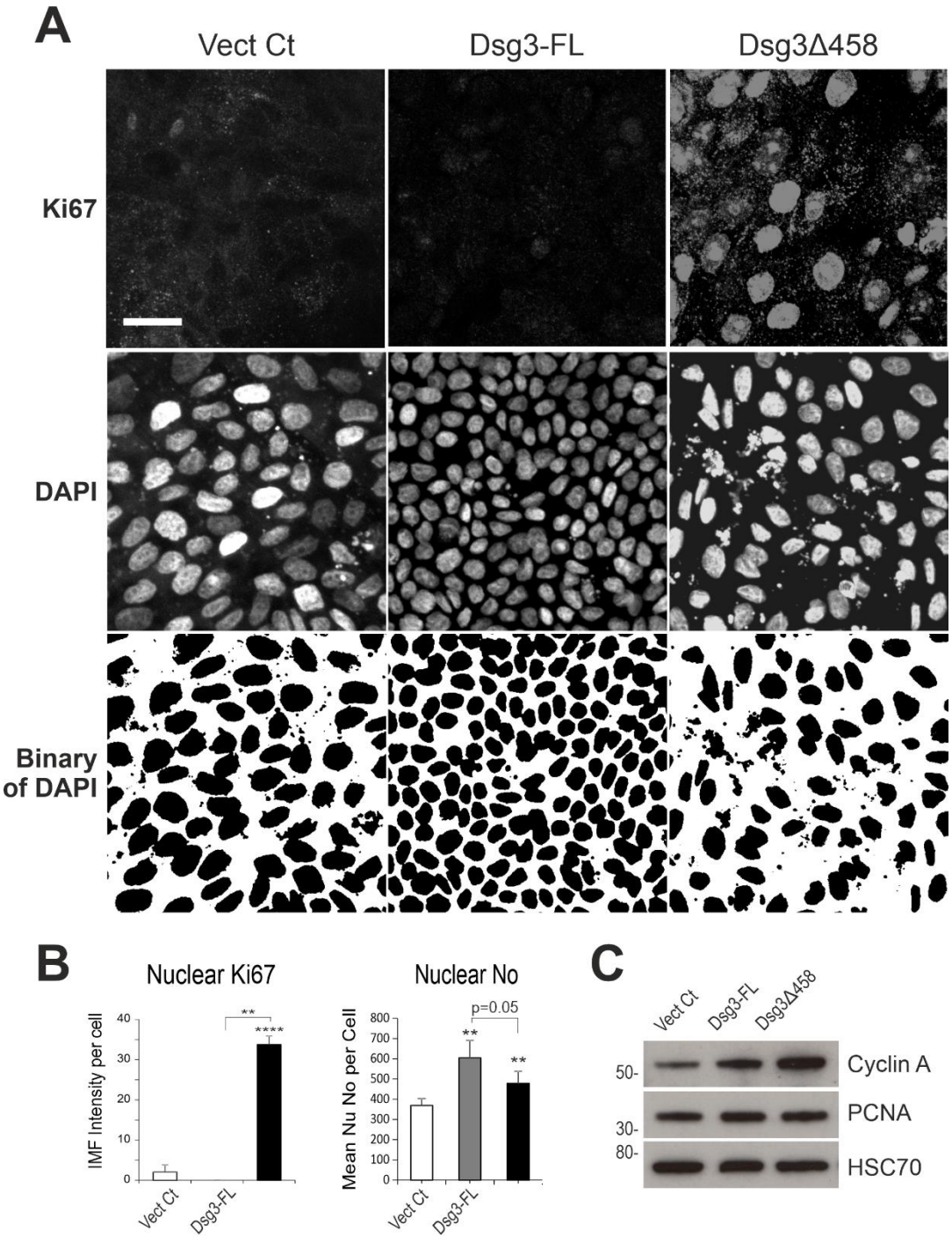
A
Vect Ct
Dsg3-FL
Dsg3Δ458
Ki67
DAPI
Binary of DAPI
B
Nuclear Ki67
IMF Intensity per cell
Vect Ct
Dsg3-FL
Nuclear No
Mean Nu No per Cell
p=0.05
C
Vect Ct
Dsg3-FL
Dsg3Δ458
50-
30-
80-
Cyclin A
PCNA
HSC70

Table 1. Summary for the phenotypes of Dsg3-FL and Dsg3ΔC cell lines

Phenotype	Assay	Dsg3-FL	Dsg3ΔC
Dome formation		↓	↑↑
ROS production		↓	↑
Apoptosis	β-gal staining	↓	↑
	Annexin V staining	↓↓	↑
	Sub-G1	—	↑
	Cleaved caspase-3 level	—	↑↑
Tight Junction	TER	↑↑↑	↑
	FITC-dextran flux	↑↑	↓
	Cytoskeleton	↓	↑↑
	ZO-1 staining	Polarised, Restricted to apical TJs	Cell split/crack, Basolateral accumulation
	ZO-1 blots	↓	↑
Cell proliferation	Ki67 staining	—	↑↑↑
	Cell number score	↑↑	↑
	Cell size	↓	↑

The increase or decrease as well as the levels of the changes for each parameter were indicated by orientation and number of the arrows relative to the respectively controls.